Meteorological Applications

RMetS Royal Meteorological Society

RESEARCH ARTICLE OPEN ACCESS

Identification and Forecasting of Typical Wind Shear and Shear Line Based on Two-Dimensional Wind Field

Anning Chen[1] | Jinlong Yuan[1,2] | Shuo Zhang[1] | Yue Liu[1] | Jiadong Hu[1] | Jiawei Qiu[1] | Haiyun Xia[1,3]

[1]The State Key Laboratory of Climate System Prediction and Risk Management (CPRM), School of Atmospheric Physics, Nanjing University of Information Science and Technology, Nanjing, China | [2]CMA Weather Modification Center, Beijing, China | [3]School of Earth and Space Science, University of Science and Technology of China, Hefei, China

Correspondence: Jinlong Yuan (yuanjinlong@nuist.edu.cn)

Received: 19 January 2026 | **Revised:** 13 July 2026 | **Accepted:** 28 July 2026

Keywords: 2D wind vector | coherent Doppler wind lidar | shear line | wind shear

ABSTRACT

The forecasting of clear-air wind shear presents a significant challenge in aviation meteorology. To improve the accuracy of wind shear identification and forecasting using coherent Doppler wind lidar, this study proposes an advanced method for identifying and forecasting wind shear and shear line. The method first performs point-by-point sliding traversal of potential wind shear along the radial and tangential direction based on retrieved two-dimensional wind vector. Subsequently, shear points are identified and extracted by the wind vector, and spatial clustering analysis is applied to reconstruct low-level wind shear line. Finally, the movement of wind shear line is forecasted with the average wind vector in the guidance region of shear line segments. This study simulated two simplified wind shear scenarios that retain key wind field features: gust front passage and divergent airflow. It compared the identification and forecasting performance of wind shear and shear line based on radial speed and two-dimensional wind vector. Results demonstrated that under controlled kinematic conditions, the two-dimensional wind vector method provides more accurate identification and improved forecast precision. The proposed method effectively identified and forecasted shear lines induced by gust front and severe convection in the airport field experiments. This study provides technical support for airport low-level wind shear early warning and flight safety assurance.

1 | Introduction

Wind shear is typically defined as a sudden, significant change in wind speed or direction either vertically or horizontally (ICAO 2005). The shear line refers to a narrow, concentrated wind shear region with wind field discontinuity (characterized by significant velocity or wind direction gradients). Wind shear, a hidden hazard for low-altitude flight, is prone to causing aircraft stalling, loss of control, and even safety accidents, posing a significant threat to civil aviation and low-altitude operations (Anthony and Derek 2019; Hallowell and Cho 2010). Low-level wind shear is characterized by small scales and rapid variations. Forecasting its movement trajectory and impact range remains challenging even if real-time signals are captured, leaving extremely limited time for aircraft adjustments. Therefore, improving the accuracy of wind shear identification and achieving effective early warning are crucial for ensuring aviation safety, reducing property losses, and enhancing flight efficiency (Nechaj et al. 2019; Borsky and Unterberger 2019).

Common atmospheric wind field detection equipment such as surface anemometers, wind profilers, Doppler weather radars, and Doppler wind lidars all provide key technical support for real-time detection of wind shear (Zrnić et al. 1985; Zhao et al. 2021; Zhao and Shan 2022; Li et al. 2020; Zhou et al. 2018; Hon and Chan 2014). Doppler weather radar can effectively detect aerosol particles within precipitation systems, offering significant advantages in identifying mesoscale shear lines such as convergence lines and fronts (Yuan et al. 2018; Hwang et al. 2017; Zheng et al. 2014). Lidar with high spatiotemporal resolution is capable of providing accurate Doppler wind measurements (Wang et al. 2024, 2021, 2025; Iwai et al. 2011), thus playing a crucial role in clear-air wind shear detection (Huang et al. 2024; Zhao et al. 2025; Zhang et al. 2019; Hon and Chan 2014). With the rapid advancement of artificial intelligence, various models have been widely applied in wind shear identification research, significantly improving the efficiency of shear line identification (Biard and Kunkel 2019; Cai et al. 2021; Tian et al. 2024). Although these technologies have achieved effective identification of low-level wind shear, research on the forecast of wind shear and shear line remains limited.

Accurate wind shear forecasting is crucial for enhancing aviation safety. Early shear line forecast methods are mostly based on numerical models, weather radar network data, and so forth, employing linear extrapolation to achieve medium-to-short-term forecasts (Qian et al. 2013; Browning et al. 1982). Machine learning algorithms demonstrate significant potential in handling complex non-linear relationships, offering a more effective technical method for shear line forecast (Liu et al. 2012; Coburn et al. 2022; Lagerquist et al. 2019; Khattak et al. 2024). However, existing studies mainly focus on shear line forecast for mesoscale systems, and exploration in the field of smaller-scale (1–20 km) clear-air shear line systems is particularly insufficient.

In previous work, effective identification of low-level wind shear and shear line was achieved by combining a dual filtering mechanism with shear points clustering analysis, enabling forecast of approximately 25 min in urban wind field (Chen et al. 2025). However, this method relies solely on radial speed data. Regions where wind shear is parallel to the lidar radial direction cannot be identified, resulting in incomplete shear line identification. Meanwhile, discrepancies exist between the radial speed and the actual horizontal wind speed, which induce positional deviations in shear line identification and thereby compromise forecast accuracy. Therefore, developing a more reliable and accurate method for wind shear and shear line identification and forecast remains an urgent challenge at this stage.

To further improve the identification accuracy and forecast precision of wind shear using lidar, this study proposes an advanced method for wind shear and shear line identification and forecast based on two-dimensional (2D) wind vector. The rest of this paper is organized as follows: Section 2 elaborates on the theoretical basis of the proposed method. Section 3 compares the wind shear identification and forecast performance of 2D wind vector versus radial speed through typical wind shear field simulations. Section 4 verifies the effectiveness of the method through airport wind shear identification and forecasting experiments. Section 5 provides discussion and conclusion. In this paper, LST (local standard time, LST = UTC + 8) is used.

2 | Method

This study proposes a method for identifying and forecasting wind shear and shear line based on 2D wind vector. It identifies potential wind shear ramps by performing point-by-point sliding traversal along the radial and tangential direction. Wind shear line is derived by extracting and clustering shear points by wind vector. Movement forecast is achieved using the average wind speed within the shear line guidance region. Figure 1 shows the flowchart of the proposed method, with the main steps summarized as follows:

Step 1. Wind shear ramps are extracted and identified using an orthogonal direction vector ramp detecting method. First, the 2D wind vector is retrieved from radial speed detected by lidar with the variational method (Chan and Shao 2007; Yuan et al. 2022). The variational method, grounded in atmospheric mass and spatial continuity, retrieves the 2D wind vector by minimizing a cost function comprising background, radial

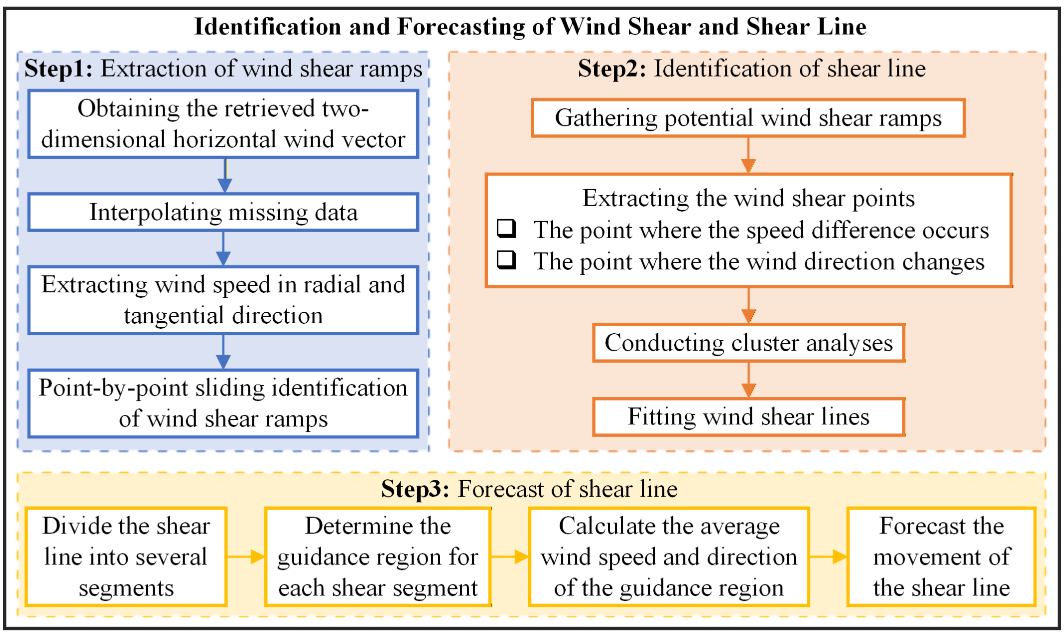

FIGURE 1 | The flowchart of wind shear and shear line identification and forecast.

observation, spatial smoothing, and momentum conservation terms. This effectively resolves the inherent ill-posed nature of wind retrieval from radial speed, ensuring the retrieved wind field is observationally consistent and physically coherent.

Due to signal attenuation in the atmospheric medium and beam blockages, wind speed data are prone to missing values, leading to data gaps or anomalies that can interfere with the identification of valid wind shear. Therefore, effective interpolation of missing data is required to enhance the accuracy of wind shear identification. Based on the K-neighborhood frequency method (Xu et al. 2023), which has been widely applied in lidar wind field quality control. Specifically, an $M \times N$ neighborhood window is centered at each missing point. All valid wind speed data within the window are divided evenly into P intervals, and the distribution frequency of each interval is calculated. Here, X_{MAX} denotes the maximum frequency among all intervals, V_P is the middle wind speed of the corresponding interval, and K serves as the triggering threshold for interpolation. Interpolation is performed only when $X_{\mathrm{MAX}} \geq K$. An excessively large K makes most missing points un-interpolatable and reduces the spatial integrity of the wind field. By contrast, an overly small K may lead to over-filling with sparse samples and introduce wind field errors. Considering the typical spatial scale of low-level wind shear and the resolution of the lidar, a 3×3 window with P set to 10 and K set to 5 (i.e., where more than 60% of the points within the window are valid) is generally considered the optimal parameter configuration. To balance the continuity of wind field characteristics with the authenticity of abrupt signal changes, data interpolation is primarily conducted in two aspects. If the variation in wind speed within the window is too great, the middle wind speed V_P is adopted for reliable interpolation; otherwise, bilinear interpolation is applied instead.

Compared to the traditional scalar ramp detecting method that identifies only in fixed directions, this study adopts an orthogonal direction vector ramp detecting method to identify potential wind shear. The 2D wind speeds are extracted along the radial and tangential directions, progressively extending the detection length from the minimum ramp length to traverse all potential wind shear ramps point-by-point. Wind shear ramps refer to distance segments with wind vector variations. The wind vector difference can be expressed as:

$$\overrightarrow{\Delta V} = \overrightarrow{V}(i+d) - \overrightarrow{V}(i) \tag{1}$$

where $\overrightarrow{\Delta V}$ is wind vector difference of wind shear ramp; i is the index for wind speed, d is the ramp detection length. In consideration of the lidar range resolution, which typically ranges from 30 to 150 m, the minimum ramp detection length d is set to 300 m as a physically constrained lower limit. The method performs a full-scale search of the wind shear ramps above minimum length. If focusing only on larger-scale wind shear events, this minimum length can be increased accordingly. The corresponding ramp magnitude ΔV is expressed as:

$$\Delta V = \left[(u(i+d) - u(i))^2 + (v(i+d) - v(i))^2 \right]^{\frac{1}{2}} \tag{2}$$

u and v are latitudinal and longitudinal wind components, which can be retrieved by the 2D variational method (Chan and Shao 2007; Yuan et al. 2022). Wind shear is essentially the spatial gradient of wind vector, whose intensity depends on both wind speed and direction differences. Compared to traditional method, this formula directly calculates wind vector difference by integrating both latitudinal and longitudinal winds, comprehensively accounting for wind shear caused by wind speed and direction discontinuities. It thus provides a more objective quantification of the true intensity of wind shear.

Step 2. Identifying wind shear line through shear points extraction and cluster analysis. Extracting shear points of all potential wind shear ramps based on wind vector. Compute the wind vector difference point-by-point, identifying the discontinuity in wind speed as shear point. If no significant wind speed abrupt change within the ramp, the wind direction abrupt change point shall be extracted using the retrieved horizontal wind direction. If neither exhibits abrupt change characteristics, the center point of the ramp is defined as the shear point.

Compared to the previous method relying solely on the sign of radial speed (positive values indicating motion toward the lidar, negative values indicating motion away from the lidar) to determine abrupt changes, this study locates shear points based on the abrupt change characteristics of 2D wind vector. It enables more accurate spatial positioning of shear points, thereby effectively enhancing the accuracy of wind shear line identification.

Wind shear with multiple scales is widely prevalent in complex atmospheric environments. Wind shear line serves as a typical wind shear system with significant spatial continuity, which is susceptible to interference from isolated or scattered wind shear during position identification. Therefore, performing cluster analysis on shear points to extract continuously distributed wind shear is crucial for identifying shear line. On the one hand, adjacent effective shear points with linear spatial characteristics are aggregated; on the other hand, it also filters out isolated noise points. The clustering algorithm is as follows: First, obtain the Cartesian position coordinates of all shear points. An initial shear point is randomly selected as the cluster center, around which a circular region with radius $R_{\min}$ (minimum distance threshold) is defined. Unclassified shear points within this region are merged into the cluster, and continue searching around each new point while excluding classified ones until all points are clustered.

After clustering analysis, the resulting clusters include not only the linear feature clusters but also invalid clusters. Firstly, a threshold for the minimum number of shear points in cluster is set to exclude small clusters. Then, the estimated curve length of each cluster is calculated using distance formula. Only linear feature clusters exceeding a preset threshold in length are selected for curve fitting, enabling the reconstruction of shear lines within the region (Chen et al. 2025). The above clustering thresholds and linear feature cluster length threshold can be flexibly adjusted according to the spatial distribution of wind shear points and research objectives. In this paper, targeting the identification of mesoscale and small-scale wind shear lines ranging from 1 to 20 km, $R_{\min}$ is set to 1 km and the minimum number of shear points in cluster is set to 15. For the identification of smaller-scale local wind shear, these thresholds can be appropriately reduced. However, the optimal thresholds need to be determined on the basis of a large number of cases.

Step 3. Movement forecast of wind shear line based on average wind vector. As a flow embedded boundary, the shear line is dynamically coupled with the background wind field. The upstream flow provides continuous momentum advection and energy transport and acts as a steering flow to govern the translation of the shear line. Therefore, its movement direction and speed are primarily determined by the stronger background wind in the upstream region. To achieve rapid short-term forecasting of shear line for airport real-time early warning, this method adopts a simplified advection assumption. It neglects the complex internal dynamic evolution of convection and only extracts the environmental wind vector behind the shear line, conducting forecasts via environmental advection extrapolation.

Notably, the actually identified wind shear line is often irregularly curved. If employing global wind field characteristic analysis, it will be difficult to accurately capture the dynamic regions driving the movement of each shear line segment. Consequently, this study adopts a segmented processing strategy, dividing the fitted wind shear line into several shear segments. For each shear segment, equal-scale rectangular regions are delineated on either side. The average wind speeds within the two regions are calculated and compared, with the side exhibiting the higher wind speed being selected as the dynamic guidance region for that shear segment.

Subsequently, the horizontal mean wind speed and direction within the guidance region are calculated. And taking them as key dynamic parameters for forecasting shear line movement, thereby enabling refined forecasting of the spatial movement trend of each shear line segment. In contrast to radial speed, which only reflects the 1D movement characteristics along the lidar detection direction, the 2D wind vector can fully characterize the true direction and velocity of the wind field. It effectively enhances the accuracy and reliability of forecast results.

The simplified advection assumption performs well in short-term forecasting of low-level wind shear dominated by environmental advection, but has limitations for self-propagating extreme convection. Such systems produce near-surface cold pools via sustained cold downdrafts. Density contrasts and buoyancy gradients between cold and warm air spread density currents outward, triggering non-advective autonomous propagation of shear lines. In such cases, shear lines advance independently of background winds, which restricts the applicability of the proposed method.

3 | Simulation and Analysis of Typical Wind Shear Line

Near-surface strong winds and divergent airflows frequently bring significant speed gradients and abrupt wind direction changes, readily inducing low-level wind shear. Characterized by high suddenness and extensive impact, these phenomena pose potential threats to aviation operations, transportation, and the safety of engineering infrastructure. To examine the performance of the proposed method, this section carries out experiments and analysis through idealized numerical simulations of typical gust front and divergent airflow passages. To rapidly construct the key structural features, simplified mathematical models are adopted for the simulations, which also match the lidar resolution.

3.1 | Identification and Forecasting of Wind Shear in Gust Passage Wind Field

To accurately capture the movement characteristics of wind shear during gust front passage, the simulated wind field comprises two components: the background wind field and the gust wind field. The background wind field is set as 3 m/s with direction of 145°. To focus on the variation of wind shear within the wind field and eliminate interference from complex factors such as surface inhomogeneity, the gust wind field is simplified during simulation. The wind direction is uniformly set as westerly across the entire gust field, while the spatial distribution of wind speed follows the characteristic of north–south symmetry and cosine attenuation from the center to the edges. Specifically, with the north–south center of the wind field as the axis of symmetry, the wind speed within the gust field is calculated using the cosine attenuation model:

$$V_s(y) = V_{\min} + \left(V_{\max} - V_{\min}\right) \cdot \frac{\cos\left(\frac{|y-y_c|}{y_{\text{half}}} \cdot \pi\alpha\right) + 1}{2} \tag{3}$$

where $V_s(y)$ is the wind speed at the ordinate y in the simulated wind field; $V_{\min}$ and $V_{\max}$ are the minimum wind speed at the north–south edges and the peak wind speed; y_c is the ordinate of the axis of symmetry; y_{half} is half the north–south span of the wind field, $y_{\text{half}} = \max\left(|y - y_c|\right)$; α is the decay coefficient. In this simulation, the peak wind speed is 20 m/s. Wind speeds at the north–south edge regions decrease to 10–11 m/s, with the decay coefficient of 0.4.

A gust field with a curved boundary (exceeding the north–south span of the simulation domain) is first initialized outside the simulation area using predefined wind field parameters. The leading-edge boundary of the gust field is represented by a series of points uniformly distributed along the y-axis. At each fixed time step, the boundary points of the gust field move independently at the corresponding wind speed and direction, which enables the gradual passage of the strong wind over the simulation domain and the dynamic evolution of its spatial coverage. The distribution of wind speed and direction within the gust field itself does not change over time during the movement. Outside the gust field, only the background wind exists, whereas inside the field, the gust wind replaces the background wind. The simplified simulation that retains key wind field features is mainly designed to verify the capability of the proposed method to identify abrupt wind field boundaries. However, the simulation is a simplified kinematic scheme. Key physical processes, including pressure-gradient forcing, density-current dynamics, turbulence, and intrinsic variability, are not incorporated in the current framework. It has limitations and cannot fully reproduce the dynamic evolution of the real atmosphere.

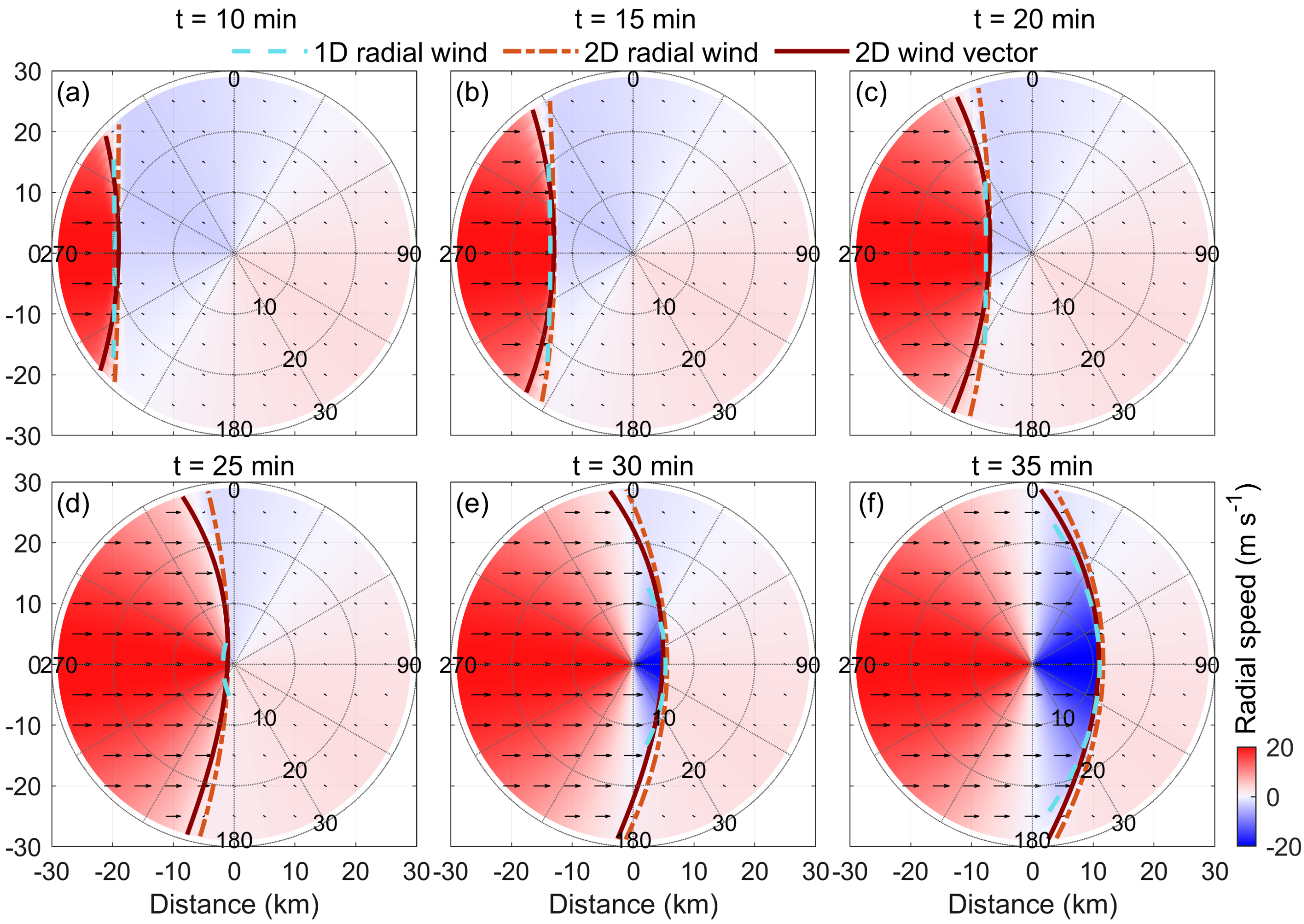

FIGURE 2 | Wind shear lines identification results of gust wind field via the 2D wind vector method, 1D and 2D radial wind methods. The background wind field is set as 3 m/s with direction of 145°.

During the validation phase of wind shear identification and forecasting, six typical times within the simulation period from $t = 10$ min to $t = 35$ min are selected for analysis. Figure 2 compares and displays the distribution results of wind shear lines obtained by the proposed 2D wind vector identification method, alongside 1D radial wind identification and 2D radial wind identification methods. Specifically, the 1D radial wind identification method only extracts wind shear information along the lidar detection radial direction, whereas the 2D radial wind identification method synchronously analyzes the radial speed variation characteristics along both the radial and tangential directions.

Due to the spatial gradient inhomogeneity of north–south wind speed decay, the wind shear lines identified by the three methods are all distinctly curved. Comparative analysis reveals that the identification results based on 2D wind vector more accurately align with the leading edge of gust front, with their shear line morphology closely matching the spatial distribution of abrupt wind field changes. In contrast, the 1D identification method relying solely on radial speed has obvious limitations, with insufficient spatial coverage of the identified wind shear lines. When the orientation of the wind shear region is consistent with the lidar detection radial direction, this method completely fails because it cannot capture the tangential wind field abrupt change signals. At this point, the 2D radial wind identification method can effectively compensate for the dimensional limitations of 1D identification. However, since radial speed data only reflect the wind field characteristics along the lidar detection direction, positional deviations exist in the identification of shear lines.

To evaluate the shear line forecasting performance of the proposed method, single-step position movement forecasts are then conducted for the shear lines identified by the three aforementioned methods. Within adjacent frames (short time intervals), the wind speed and direction of the wind field exhibit small variations. The shear line position at the subsequent time step is forecasted based on its previous position and the associated wind field characteristics, with a forecast lead time of 5 min in this case. The points upper, middle, and lower on the wind shear line identified by the 2D wind vector method are selected as target points according to the length ratio. The point on the forecasted shear line with the nearest Euclidean distance to each characteristic point is taken as its forecasted position, ensuring one-to-one correspondence. Figure 3 comprehensively presents the forecast results of the upper, middle, and lower points on the shear lines derived from the three aforementioned methods. It is shown that the shear line identified by the 2D wind vector method matches well with the preset gust wind fields. Forecast results indicate that the trajectories of characteristic points generated by the 2D wind vector method largely coincide with the target points,

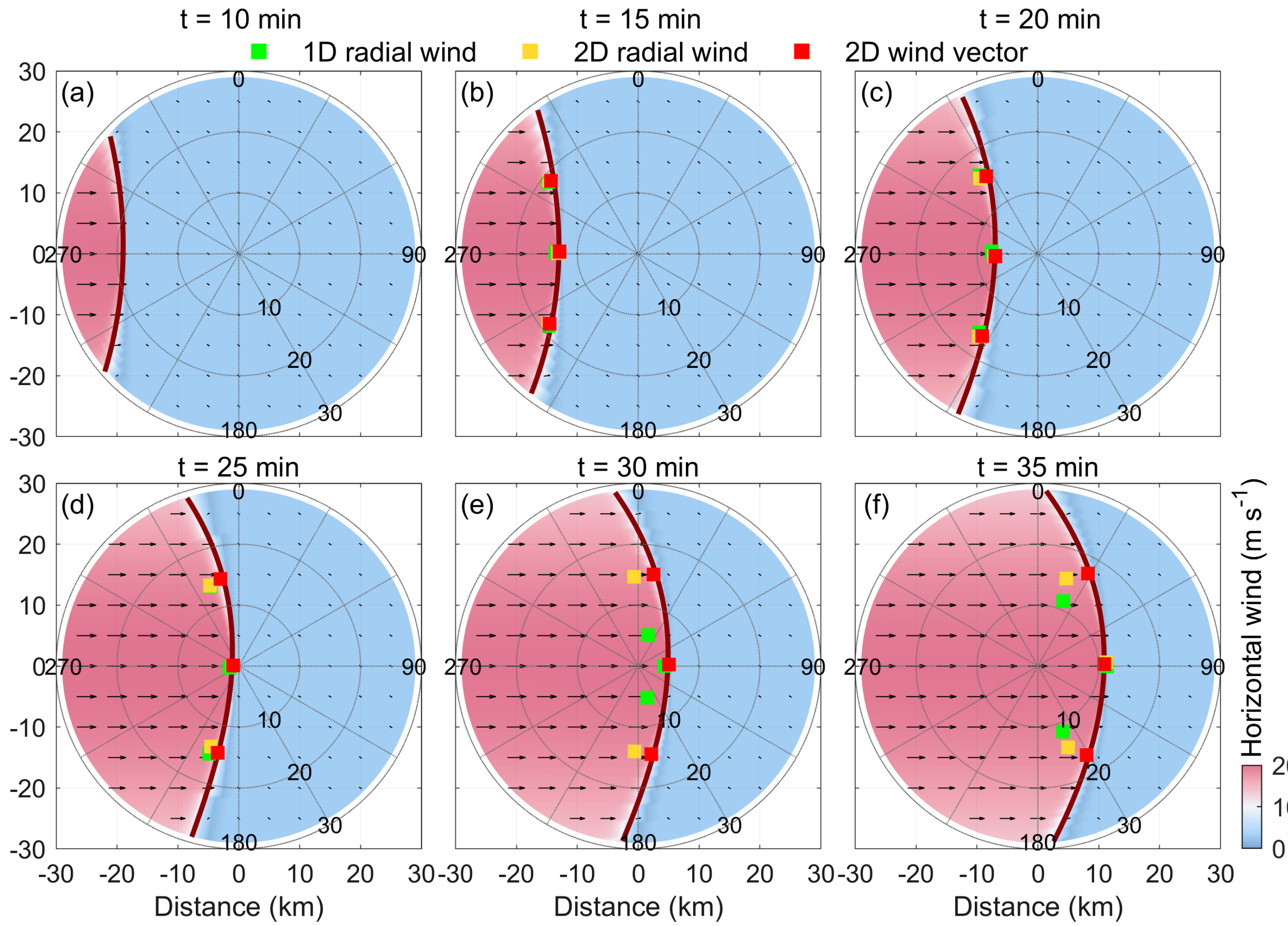

FIGURE 3 | Forecast results of gust wind field for upper, middle and lower points of wind shear lines based on three methods. (a)–(f) The forecast results via the 2D wind vector method, 1D and 2D radial wind methods at six consecutive times, respectively. The red curves in the figure represent the wind shear lines identified using the 2D wind vector method.

TABLE 1 | Forecast mean positional error in gust wind field based on the three methods.

Simulation time, *t* (min)	1D radial wind (km)	2D radial wind (km)	2D wind vector (km)
15	0.66	0.61	0.31
20	0.96	0.73	0.25
25	1.44	1.40	0.24
30	6.71	2.31	0.31
35	4.14	2.72	0.26
Mean error	2.78	1.55	0.27

demonstrating significantly superior forecasting performance compared to the two radial wind speed-based methods. In contrast, both the 1D and 2D forecast results based on radial speed exhibit varying degrees of lag, failing to accurately capture the real-time progression of the shear lines.

To quantitatively describe the forecasting performance of each method, the mean positional error of forecasts based on the three methods is statistically calculated at each time point, with the results presented in Table 1. For a given forecast method, Euclidean distances between target and forecast positions of each characteristic point are calculated at each time step. The positional errors of the three points are averaged to yield the mean deviation at that moment, and the average over all time steps gives the final mean positional error of the method. As indicated in the table, throughout the entire forecast process, the positional errors of the 2D wind vector-based method are significantly smaller than those of the radial speed-based methods, with an average positional error of merely 0.27 km. Meanwhile, the limitations of the 1D radial wind method are further amplified during the forecast process. Owing to incomplete identification of the shear lines, this method yielded the largest overall positional deviations, with a mean error of 2.78 km and a maximum error of up to 6.71 km.

Meanwhile, to further validate the forecast performance based on 2D horizontal wind vector, single-step time forecast experiments are conducted for three characteristic points along the shear line, which aim to accurately forecast the arrival times at the next position. Figure 4 displays the forecasted arrival times and corresponding time errors for the three points, where positive errors indicate early arrival and negative errors indicate delayed arrival relative to identifications. Under the stable

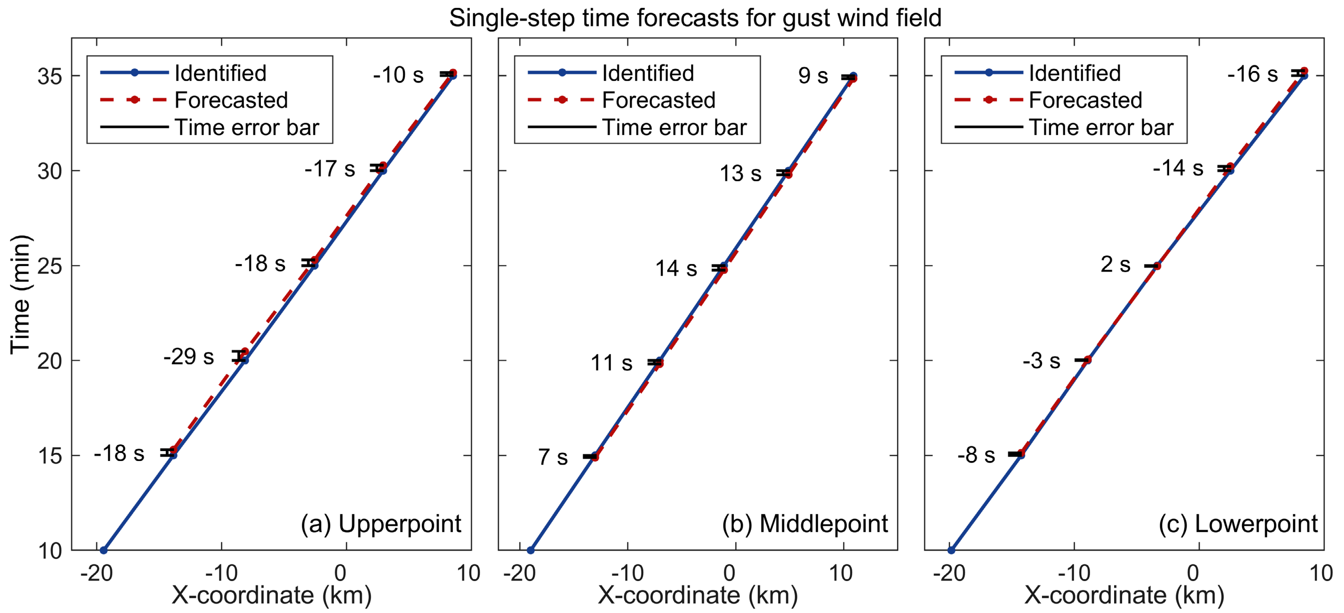

FIGURE 4 | Single-step time forecasts for gust wind field and identification results of characteristic points using 2D wind vector. (a)–(c) The time forecast results and time errors for the upper, middle, and lower points along the shear line respectively. Red dots denote forecast times, while blue dots indicate the arrival times of identified shear lines. The horizontal axis represents the *x*-coordinate of each characteristic point.

simulated wind field conditions, the time errors of the single-step forecasts are on the order of seconds, with a maximum error of only −29 s.

3.2 | Identification and Forecasting of Wind Shear in Divergent Airflow Wind Field

To verify the reliability of the proposed method in divergent wind fields, this study also constructs a numerical divergent airflow field, where the speed is set to be constant across the entire field and the wind direction exhibits radial divergence. In the simulation process, the divergence source is fixed outside the western boundary of the simulation domain, and a semicircular wind field model (covering an azimuth range of $\pm 90^{\circ}$) is adopted. The divergent wind vector satisfies the following distribution law:

$$\begin{cases} v_x(r,\beta) = v_g \cos\beta \\ v_y(r,\beta) = v_g \sin\beta \end{cases} \tag{4}$$

where v_x and v_y denote the zonal and meridional components of the divergent wind; $v_g = 15\,\mathrm{m/s}$ is the constant divergent wind speed in the wind field; r is the straight-line distance from the grid points to the divergence source within the simulation domain; β is the azimuth of the grid points relative to the divergence source in the simulation domain, $\beta \in \left[-90^{\circ}, 90^{\circ}\right]$.

Figure 5 presents the distribution results of wind shear lines obtained via the 2D wind vector method, the 1D and 2D radial wind identification methods at six typical times within the simulation period of $t = 10$–35 min. During the 2D radial-tangential identification process, shear points are identified not only by radial speed signs but also by retrieved wind directions to locate the positions of direction changes. Although this method effectively captures the wind direction variations in the divergent wind field, the deviation between radial and actual wind speeds still leads to discrepancies between the fitted shear lines and the true boundaries of the divergent airflow field. The limitations of the 1D radial identification method are particularly pronounced in this wind field. As the core shear source here is characterized by abrupt wind direction changes, reliance solely on radial-dimension identification fails to capture tangential wind direction change signals. Consequently, the shear lines identified remain incomplete throughout the period $t = 10$–25 min.

In this experiment, the upper, middle, and lower points of the shear line identified by the 2D wind vector method are also selected as target points to compare the forecast accuracy of multiple methods. Figure 6 presents the forecast results of the three methods in the divergent airflow field. It can be observed that the radial speed-based methods (1D and 2D) still exhibit significant forecast deviations. As shown in Figure 5, under the setting of "constant wind speed" in the divergent airflow field, there exists a distinct radial speed zero-value zone in the field. This characteristic can substantially interfere with the movement forecast of the shear line derived from radial speed, thereby significantly reducing the forecast accuracy. The forecasting deviation of the 1D radial identification method is most pronounced. Constrained by the insufficient integrity of the identified shear lines, its forecast points consistently exhibit a distribution characteristic of "lag + deviation".

Table 2 presents the forecast mean positional errors of the three methods at each time point. As indicated in the table, the 2D wind vector-based forecast method still demonstrates distinct advantages in the divergent airflow field. The forecast errors of the radial speed-based methods are comparable to those obtained in the gust wind field, with deviations at certain times even slightly exceeding those of the gust field. This fully demonstrates that methods relying solely on radial speed are incapable of accurately capturing the characteristics of speed variations within wind fields, nor can they effectively capture sudden changes in wind direction. Such methods exhibit significant

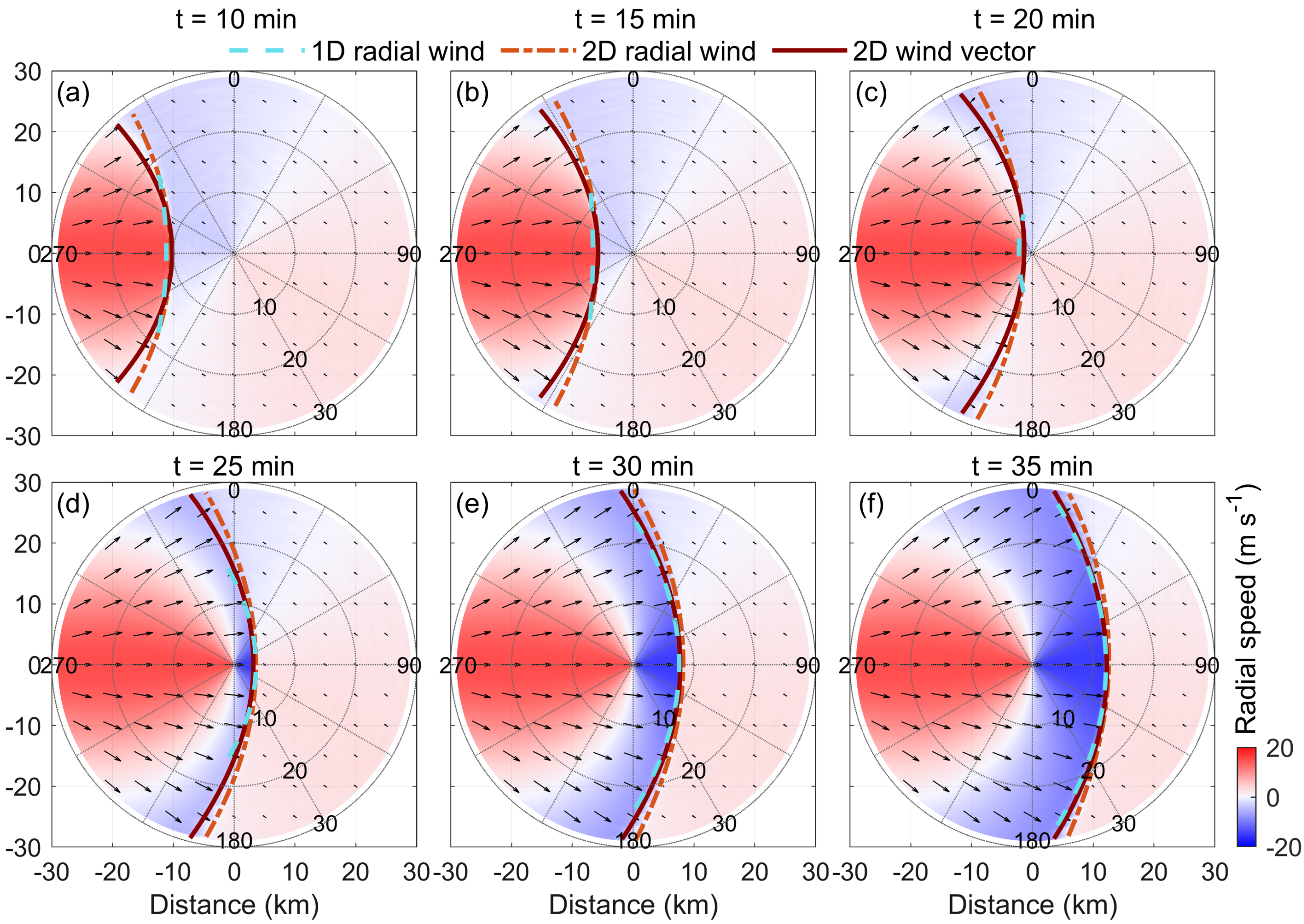

FIGURE 5 | Wind shear lines identification results of divergent wind field via the 2D wind vector method, 1D and 2D radial wind methods. The background wind field is set as 3 m/s with a direction of 145°.

limitations in wind shear scenarios coupled with both speed and wind direction gradients.

The "constant wind speed" setting in the divergent airflow field eliminates the interference of speed gradients on forecast, retaining only the influence of wind direction factors. The forecast accuracy of the 2D wind vector method is generally superior to that obtained in the gust wind field, with a minimum positional error as low as 0.07 km and an average error of 0.13 km.

Figure 7 illustrates the single-step time forecast results and time errors for the upper, middle, and lower points using a 2D wind vector. The time errors of the upper point (Figure 7a) and middle point (Figure 7b) on the shear line predominantly exhibit "positive bias", while the lower point (Figure 7c) shows "negative bias" (forecast lag). Overall errors are similarly slightly smaller than those in the gust field, with a maximum time error of 21 s and an average time forecast error across all three points of 10 s. It validates the capability of the proposed method to accurately capture wind direction characteristics.

Combining the experimental results of the two simulated wind fields, the 2D wind vector method simultaneously captures wind speed and wind direction shear information. It not only addresses the limitations of 1D identification in terms of completeness but also enables precise identification of the boundaries where wind fields abruptly change, achieving an accurate fit to the shear line. The radial speed is essentially the projection component of the actual horizontal wind vector onto the lidar detection radial direction, with its magnitude being less than or equal to the magnitude of the horizontal wind vector. Methods relying solely on radial speed remain inadequate for accurately extracting the true dynamic parameters driving shear line movement, thus markedly impairing forecast precision. In contrast, the 2D wind vector method can provide the actual velocity and direction basis for shear line movement, realize the precise movement forecast of characteristic points, and thus enhance the reliability of forecast results.

4 | Identification and Forecasting of Airport Wind Shear

Wind shear detection experiments were conducted at both Beijing Daxing International Airport (BDIA) (Yuan et al. 2022) and Kunming Changshui International Airport (KCIA), China (Xia et al. 2024). To verify the applicability of the proposed method, this study also selected and analyzed a gust event at BDIA and a severe convective weather process at KCIA, respectively.

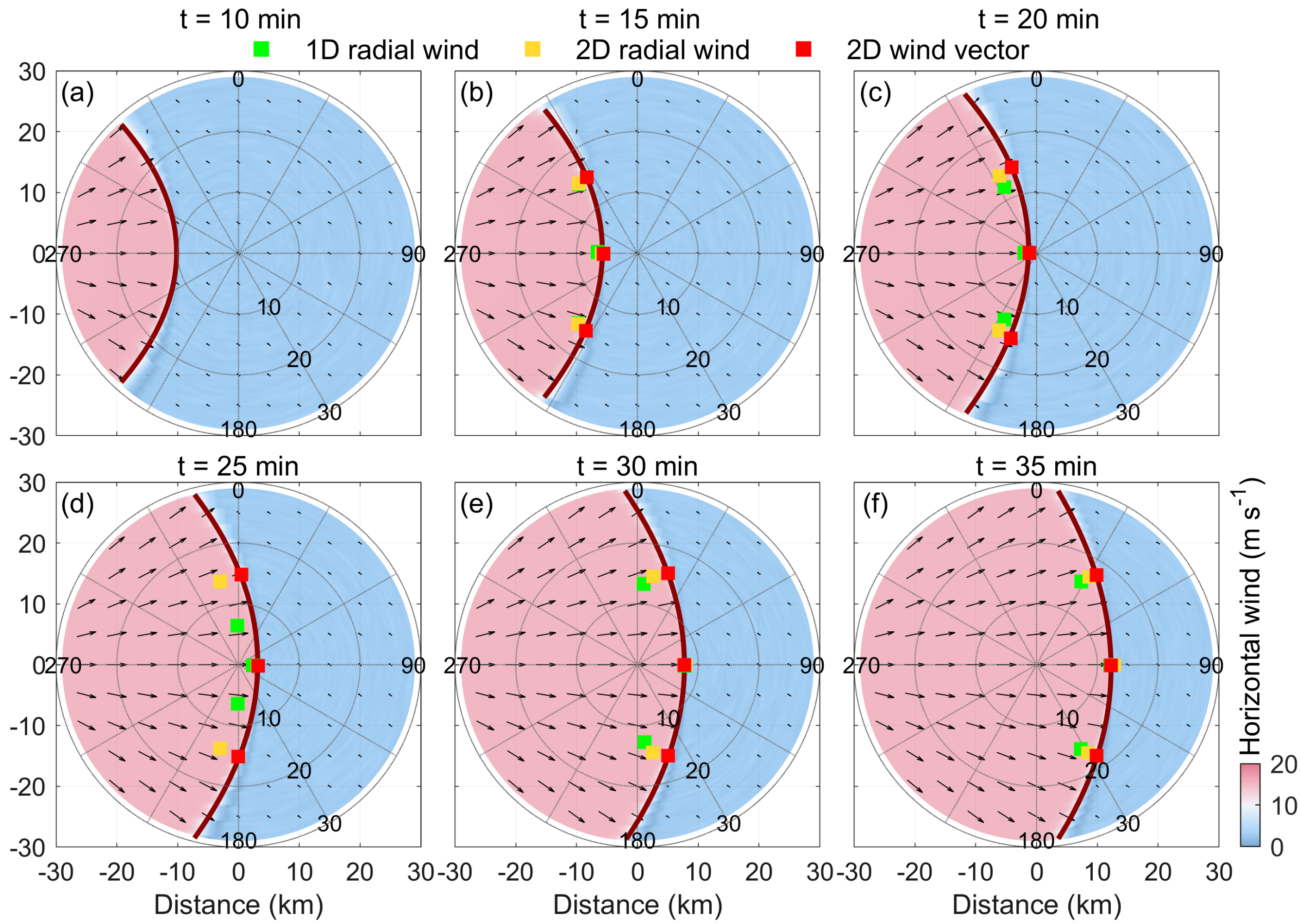

FIGURE 6 | Forecast results of divergent wind field for upper, middle and lower points of wind shear lines based on three methods. (a)–(f) The forecast results via the 2D wind vector method, 1D and 2D radial wind methods at six consecutive times, respectively. The red curves in the figure represent the wind shear lines identified using the 2D wind vector method.

TABLE 2 | Forecast mean positional error in divergent wind field based on the three methods.

Simulation time, *t* (min)	1D radial wind (km)	2D radial wind (km)	2D wind vector (km)
15	1.45	1.10	0.15
20	2.40	1.53	0.17
25	5.97	2.32	0.15
30	3.01	1.77	0.07
35	1.92	1.09	0.09
Mean error	2.95	1.56	0.13

4.1 | Experimental Results

Figure 8 presents the retrieved 2D wind vector results, as well as the wind shear line identification and forecast results at different times during a gust event at BDIA. The wind shear identification results show that at 10:12 LST on 7 July 2021, a strong southerly wind occurred over the southern part of the airport, with a maximum horizontal wind speed of approximately 10 m/s. A distinct wind shear line was detected at a distance of about 8 km from the lidar. At 10:22 LST, this shear line advanced toward the lidar to the location near 4 km, and the wind speed at the gust front exhibited attenuation. Subsequently, at 10:33 LST, the shear line moved further to the vicinity of the lidar, with the front wind speed rebounding to around 8 m/s.

During shear line forecasting, the overall movement of the shear line was forecasted by calculating the mean wind vector within the guidance regions. According to Figure 8, the forecasted and identified movement paths are basically consistent. However, there is certain deviation between the two in terms of the impact range of the shear line affected by the variability of the atmospheric wind field. The mean absolute error (MAE) between the forecast and identified shear lines was calculated, which provides a comprehensive and quantitative evaluation of the spatial error features. Since the forecast and identified shear lines often differ in length, the MAE was calculated by taking the shorter line as a reference and extracting the nearest segment with equal length from the longer one. The first forecast (Figure 8b) agreed well with the identified shear line, yielding a MAE of merely 0.19 km. The second forecast (Figure 8c) exhibited a larger discrepancy, resulting in a MAE of about 2.16 km.

The data in Table 3 demonstrate the forecast performance of the shear line based on the 2D wind vector at each time. At 10:22 LST, the coordinate of nearest point to the lidar on the forecasted shear line was (0.37, −3.86) km, with a positional error of 0.73 km from the corresponding point on the identified shear line. At this moment, the forecasted position was 3.88 km away from the

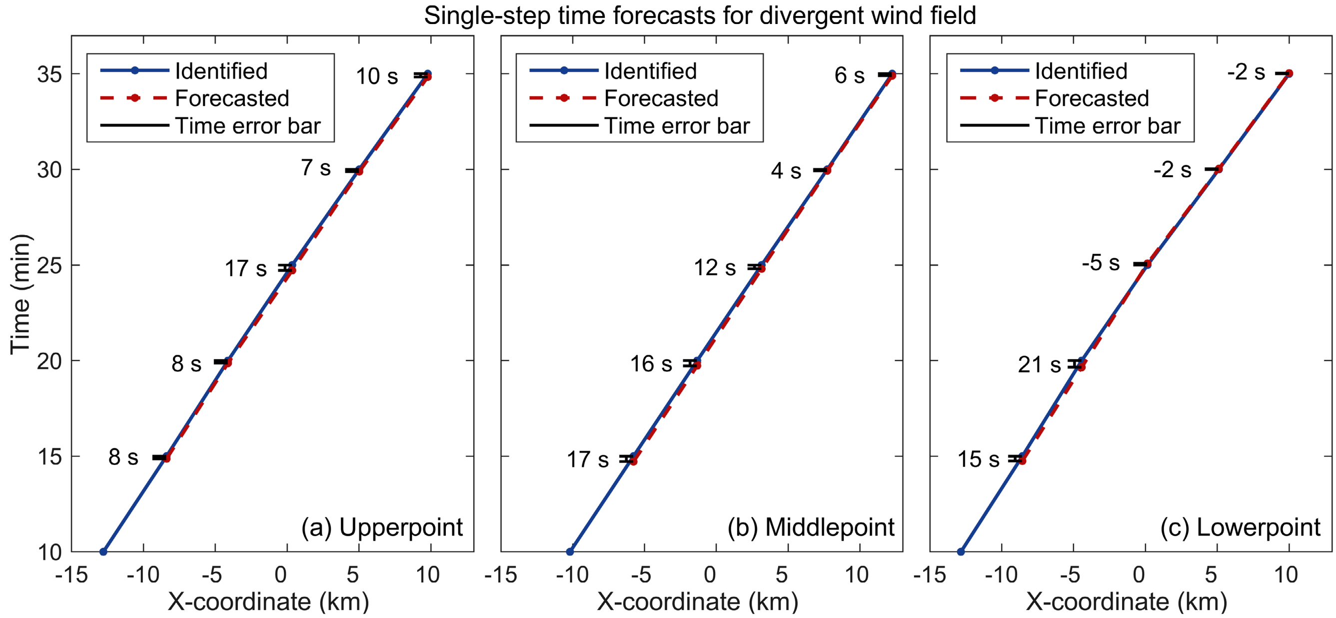

FIGURE 7 | Single-step time forecasts for divergent wind field and identification results of characteristic points using 2D wind vector. (a)–(c) The time forecast results and time errors for the upper, middle, and lower points along the shear line respectively. Red dots denote forecast times, while blue dots indicate the arrival times of identified shear lines. The horizontal axis represents the *x*-coordinate of each characteristic point.

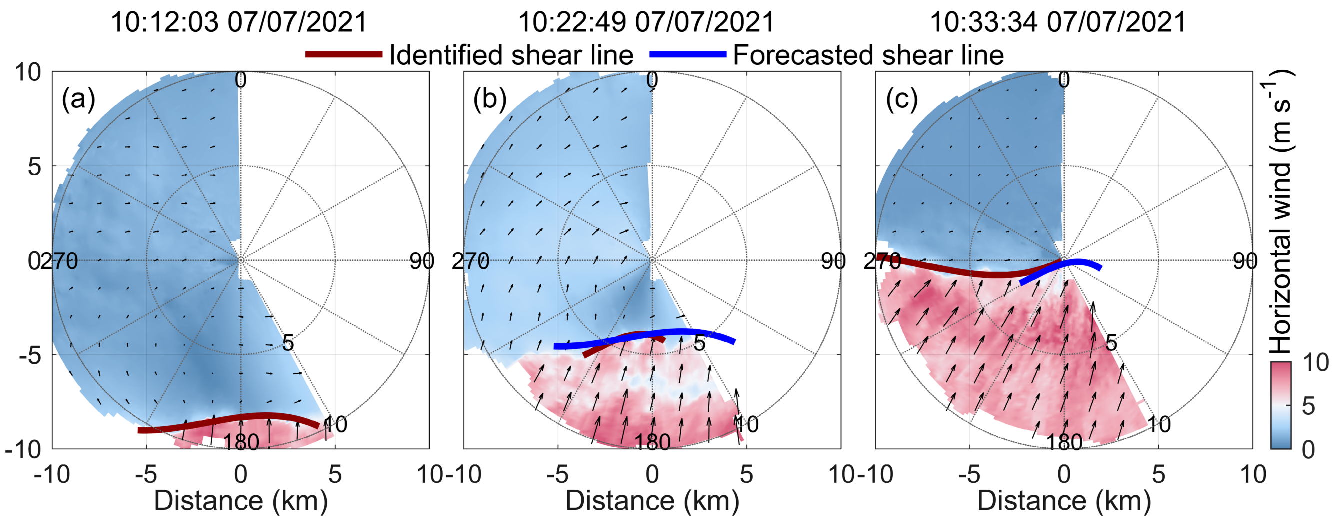

FIGURE 8 | Identification and forecast results of wind shear lines during a gusty event at BDIA. (a)–(c) The 2D wind vector results, wind shear line identification, and forecast results at different times.

TABLE 3 | Forecasting performance of shear lines based on 2D wind vector for gust event at BDIA.

Local standard time	Actual nearest point (km)	Forecast nearest point (km)	Position error (km)	Actual distance (km)	Forecast distance (km)	Distance error (km)
10:12:03	(0.63, −8.27)			8.29		
10:22:49	(−0.36, −3.93)	(0.37, −3.86)	0.73	3.95	3.88	0.07
10:33:34	(−0.14, −0.04)	(0.06, −0.18)	0.23	0.15	0.19	0.04
Mean error			0.48			0.06

lidar, with an error of merely 0.07 km relative to the actual distance. At 10:33 LST, the forecasted shear line also advanced to the vicinity of the lidar, 0.19 km away from it, with a lag of only 0.04 km compared with the identified position. Throughout the entire forecast process, the mean positional error of the nearest point to the lidar on the shear line was 0.48 km, and the mean distance error relative to the lidar was 0.06 km.

The coordinate of the point on the identified shear line nearest to the lidar was (−0.36, −3.93) km at 10:22 LST. Using this point as the target, the experiment forecasted the time to reach this location using the previously identified shear line at 10:12 LST, with a time error of only 11 s. Similarly, when using data at 10:22 LST to forecast the arrival time at the next position, the time error was about 30 s. These preliminary results indicate that the proposed method can effectively capture wind field characteristics and provide relatively accurate forecasts of shear line movement trends.

Figure 9 presents the retrieved 2D wind vector results, as well as the wind shear line identification and forecast results at different times during a severe convective event on 4 July 2022, at KCIA. During this weather process, there existed intense downdrafts over the northern area of the airport, with the maximum divergent wind speed reaching approximately 12–13 m/s. The results at 15:36 LST indicated that a wind shear line was present approximately 8 km north of the lidar, and it advanced to a location near 5 km at 15:45 LST. At 15:59 LST, the shear line had moved to the vicinity of the lidar, with the divergent wind speed weakened.

In the initial stage, owing to the relative stability of the divergent airflow, the affected regions of the forecasted and identified results at 15:45 LST were highly consistent, with a MAE of approximately 0.35 km. By 15:59 LST, a distinct positional deviation emerged between the forecasted and identified shear lines, with the MAE reaching approximately 4.14 km. It is due to the obstruction effect, whereby only the shear lines in the region to the left of the lidar can be identified, with a detection blind spot existing in the right-hand region. At this point, the forecast method based on 2D wind vector can overcome the limitations of the detection range, reconstructing the movement trends of shear lines within the undetected blank zone.

The data in Table 4 quantitatively characterize the forecast accuracy of the shear line derived from the 2D wind vector method at each time during the forecasting process. Owing to the instantaneous variability of severe convective weather, the overall forecast error is slightly higher than that obtained at BDIA, with the positional forecast exhibiting both leading and lagging characteristics. Throughout the forecast, the spatial mean positional error of the nearest point to the lidar on the shear line was 0.48 km, and the mean distance error relative to the lidar was 0.37 km.

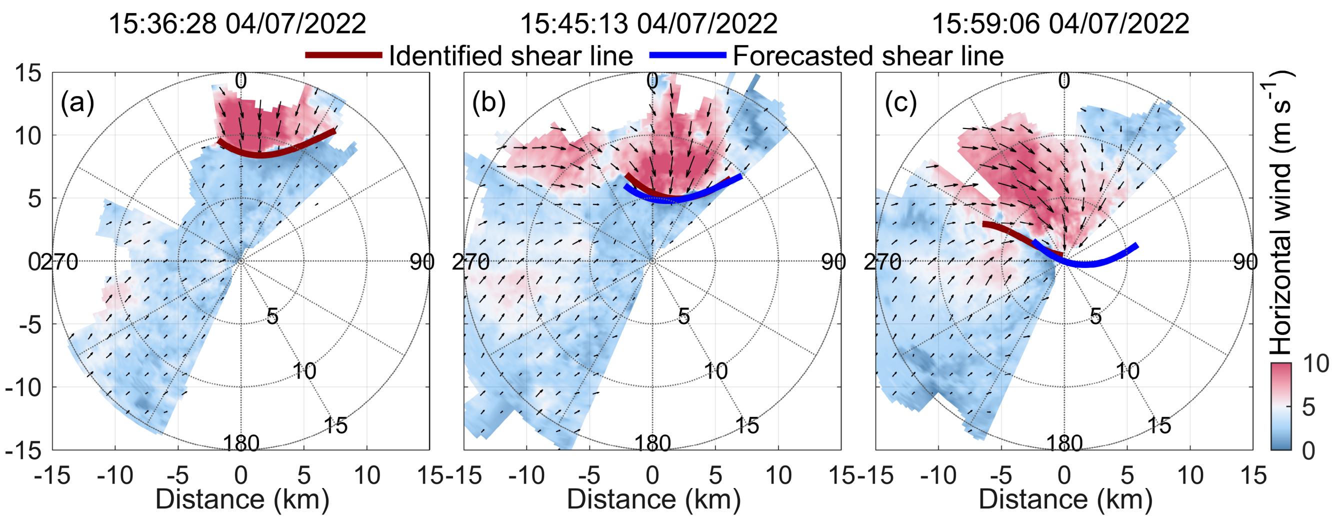

FIGURE 9 | Identification and forecast results of wind shear lines during severe convective weather at KCIA. (a)–(c) The 2D wind vector results, wind shear line identification, and forecast results at different times.

TABLE 4 | Forecasting performance of shear lines based on 2D wind vector for convective weather at KCIA.

Local standard time	Actual nearest point (km)	Forecast nearest point (km)	Position error (km)	Actual distance (km)	Forecast distance (km)	Distance error (km)
15:36:28	(0.99, 8.42)			8.48		
15:45:13	(1.01, 5.07)	(0.59, 4.82)	0.49	5.17	4.85	0.32
15:59:06	(−0.11, 0.43)	(0.01, −0.03)	0.47	0.45	0.03	0.42
Mean error			0.48			0.37

In this case, based on the shear line position and wind field at 15:36 LST, the shear line was forecast to reach the target point (1.01, 5.07) km at 15:44 LST, while it actually arrived at 15:45 LST. Thus, the corresponding forecast error was 1 min. In the same way, the forecast based on the results at 15:45 LST exhibited a time error of approximately 2 min.

4.2 | Overall Error Analysis

To comprehensively evaluate forecast performance and deviation characteristics, all forecasts from two airport experiments were integrated to quantitatively analyze the coordinate deviations along the *X* and *Y* directions between forecasted and identified shear lines. Calculations showed that the average deviation in the X coordinates of the forecasted and identified shear lines was 0.02 km, with a standard deviation of 0.09 km, representing small overall errors. The mean deviation of the Y coordinate was −0.30 km with a standard deviation of 3.45 km, indicating obvious fluctuations in positional errors.

In these cases, the shear lines all moved in a north–south direction. Therefore, positional errors of the shear lines were mainly concentrated in the *Y* direction, driven by uncertainties under complex atmospheric conditions. In contrast, the forecasted shear lines achieved good overall positioning accuracy in the horizontal *X* direction. Such deviations were mainly caused by lidar obstruction and detection gaps, which led to positioning errors when identifying shear lines.

5 | Discussion and Conclusion

This study proposes an advanced method for identifying and forecasting wind shear and shear line using 2D wind vector by lidar. Numerical simulations under controlled kinematic conditions demonstrate that the proposed method can effectively identify idealized abrupt wind field boundaries, showing improved identification and forecast performance compared with 1D and 2D radial wind methods. Radial speed-based forecasts exhibit varying degrees of lag, whereas the forecast trajectories derived from 2D wind vector are highly consistent with the actual movement of simulated wind fields. Airport experiments successfully identify shear lines induced by gust front and severe convection and achieve shear lines movement forecast.

This method achieves better localization of wind shear through orthogonal direction vector ramp detecting method, thereby more accurately representing wind shear intensity compared to conventional scalar ramp detecting method. Complete 2D wind vector information reflects the authentic characteristics of the wind field. On the one hand, it provides a reliable basis for the accurate extraction of shear points, thereby improving the accuracy of shear line identification. On the other hand, it supplies key dynamic parameters for wind shear line movement forecast, resulting in more precise forecasting outcomes. Therefore, this method offers new idea for identifying and forecasting smaller-scale wind shear line. This not only facilitates comprehensive dynamic tracking of wind shear lines but also enhances safety assurance capabilities for low-altitude flights.

Although this study has achieved preliminary results, several limitations remain to be addressed. A simplified simulation is adopted for method validation; future work will incorporate key atmospheric processes to enhance the physical realism. More observational datasets are required to support parameter sensitivity tests, comprehensive statistical analysis and validation, thereby enabling further method optimization. The performance of the method highly relies on the retrieval accuracy of the 2D wind field. The detection range of lidar is constrained by obstacle occlusion (Yang et al. 2024), which impairs its coverage capability for full-region wind field. Especially in complex terrain (e.g., mountainous and valley areas), the accuracy of 2D wind field retrieval based on single Doppler lidar observations is limited, impairing the stability of shear line forecasts. Therefore, dual- or multi-lidar networking observations are necessary to provide more complete and reliable wind fields. Meanwhile, its limited radial resolution and scanning frequency make it difficult to capture rapid changes of wind shear lines under complex weather conditions, thereby exacerbating forecast errors. Future research requires the integration of multi-source detection equipment to conduct collaborative observations. In addition, the random perturbations of atmospheric turbulence induce nonlinear variations in wind fields, which significantly reduce forecast accuracy. Turbulence parameterization should be incorporated to optimize the forecast method, further enhancing the robustness of the method.

Author Contributions

Anning Chen: validation, visualization, writing – original draft, methodology, writing – review and editing, conceptualization. **Jiawei Qiu:** conceptualization, writing – review and editing. **Shuo Zhang:** validation, methodology, writing – review and editing. **Jinlong Yuan:** conceptualization, funding acquisition, methodology, supervision, writing – review and editing. **Jiadong Hu:** conceptualization, writing – review and editing. **Yue Liu:** methodology, validation, writing – review and editing. **Haiyun Xia:** conceptualization, writing – review and editing.

Funding

This work was financially supported by the Project of the National Key Laboratory of Climate System Prediction and Change Response (CPRM-2025-NUIST-012), the Natural Science Foundation of Jiangsu Province (BK20230434), and the National Natural Science Foundation of China (42405137).

Conflicts of Interest

The authors declare no conflicts of interest.

Data Availability Statement

The data that support the findings of this study are available from the corresponding author upon reasonable request.

References

Anthony, O. C., and K. Derek. 2019. “Low Level Turbulence Detection for Airports.” *International Journal of Aviation, Aeronautics, and Aerospace* 6: 1302.

Biard, J. C., and K. E. Kunkel. 2019. “Automated Detection of Weather Fronts Using a Deep Learning Neural Network.” *Advances in Statistical Climatology, Meteorology and Oceanography* 5: 147–160.

Borsky, S., and C. Unterberger. 2019. "Bad Weather and Flight Delays: The Impact of Sudden and Slow Onset Weather Events." *Economics of Transportation* 18: 10–26.

Browning, K. A., C. G. Collier, P. R. Larke, P. Menmuir, G. A. Monk, and R. G. Owens. 1982. "On the Forecasting of Frontal Rain Using a Weather Radar Network." *Monthly Weather Review* 110: 534–552.

Cai, Y., Q. Li, Y. Fan, L. Zhang, H. Huang, and X. Ding. 2021. "An Automatic Trough Line Identification Method Based on Improved UNet." *Atmospheric Research* 264: 105839–105852.

Chan, P. W., and A. M. Shao. 2007. "Depiction of Complex Airflow Near Hong Kong International Airport Using a Doppler LIDAR With a Two-Dimensional Wind Retrieval Technique." *Meteorologische Zeitschrift* 16: 491–504.

Chen, A., J. Yuan, H. Yang, et al. 2025. "Identification and Forecasting of Low-Level Wind Shear Based on Long Range Doppler Wind Lidar." *Atmospheric Research* 330: 108558.

Coburn, J., J. Arnheim, and S. C. Pryor. 2022. "Short-Term Forecasting of Wind Gusts at Airports Across CONUS Using Machine Learning." *Earth and Space Science* 9: e2022EA002486.

Hallowell, R. G., and J. Y. N. Cho. 2010. "Wind-Shear System Cost–Benefit Analysis." *Lincoln Laboratory Journal* 18: 47–68.

Hon, K. K., and P. W. Chan. 2014. "Application of LIDAR-Derived Eddy Dissipation Rate Profiles in Low-Level Wind Shear and Turbulence Alerts at Hong Kong International Airport." *Meteorological Applications* 21: 74–85.

Huang, X., J. Zheng, A. Shao, D. Xu, W. Tian, and J. Li. 2024. "Study of Low-Level Wind Shear at a Qinghai-Tibetan Plateau Airport." *Atmospheric Research* 311: 107680.

Hwang, Y., T.-Y. Yu, V. Lakshmanan, D. M. Kingfield, D.-I. Lee, and C.-H. You. 2017. "Neuro-Fuzzy Gust Front Detection Algorithm With S-Band Polarimetric Radar." *IEEE Transactions on Geoscience and Remote Sensing* 55: 1618–1628.

ICAO. 2005. *Manual on Low-Level Wind Shear*. International Civil Aviation Organization.

Iwai, H., Y. Murayama, S. Ishii, K. Mizutani, Y. Ohno, and T. Hashiguchi. 2011. "Strong Updraft at a Sea-Breeze Front and Associated Vertical Transport of Near-Surface Dense Aerosol Observed by Doppler Lidar and Ceilometer." *Boundary-Layer Meteorology* 141: 117–142.

Khattak, A., J. Zhang, P.-W. Chan, and F. Chen. 2024. "Assessment of Wind Shear Severity in Airport Runway Vicinity Using Interpretable TabNet Approach and Doppler LiDAR Data." *Applied Artificial Intelligence* 38: 2302227.

Lagerquist, R., A. McGovern, and D. J. Gagne Ii. 2019. "Deep Learning for Spatially Explicit Prediction of Synoptic-Scale Fronts." *Weather and Forecasting* 34: 1137–1160.

Li, L., A. Shao, K. Zhang, N. Ding, and P.-W. Chan. 2020. "Low-Level Wind Shear Characteristics and Lidar-Based Alerting at Lanzhou Zhongchuan International Airport, China." *Journal of Meteorological Research* 34: 633–645.

Liu, J. N. K., K. M. Kwong, and P. W. Chan. 2012. "Chaotic Oscillatory-Based Neural Network for Wind Shear and Turbulence Forecast With LiDAR Data." *IEEE Transactions on Systems, Man, and Cybernetics, Part C (Applications and Reviews)* 42: 1412–1423.

Nechaj, P., L. Gaál, J. Bartok, et al. 2019. "Monitoring of Low-Level Wind Shear by Ground-Based 3D Lidar for Increased Flight Safety, Protection of Human Lives and Health." *International Journal of Environmental Research and Public Health* 16: 4584–4609.

Qian, W., J. Li, and X. Shan. 2013. "Application of Synoptic-Scale Anomalous Winds Predicted by Medium-Range Weather Forecast Models on the Regional Heavy Rainfall in China in 2010." *Science China Earth Sciences* 56: 1059–1070.

Tian, H., Z. Hu, F. Wang, P. Xie, F. Xu, and L. Leng. 2024. "Radar Echo Recognition of Gust Front Based on Deep Learning." *Remote Sensing* 16: 439–451.

Wang, L., F. He, J. Yuan, et al. 2025. "A Robust Threshold Method of Mixed Layer Height Based on Lidar Turbulence Data Under Different Thermal Convection Conditions." *Boundary-Layer Meteorology* 191: 32.

Wang, L., W. Qiang, H. Xia, T. Wei, J. Yuan, and P. Jiang. 2021. "Robust Solution for Boundary Layer Height Detections With Coherent Doppler Wind Lidar." *Advances in Atmospheric Sciences* 38: 1920–1928.

Wang, M., T. Wei, S. Lolli, et al. 2024. "A Long-Term Doppler Wind LiDAR Study of Heavy Pollution Episodes in Western Yangtze River Delta Region, China." *Atmospheric Research* 310: 107616.

Xia, H., Y. Chen, J. Yuan, et al. 2024. "Windshear Detection in Rain Using a 30 Km Radius Coherent Doppler Wind Lidar at Mega Airport in Plateau." *Remote Sensing* 16: 924–936.

Xu, T., X. Ma, Q. Li, and Y. Lu. 2023. "Application of Low-Altitude Wind Shear Recognition Algorithm and Laser Wind Radar in Aviation Meteorological Services." *Open Physics* 21: 154.

Yang, H., J. Yuan, L. Guan, L. Su, T. Wei, and H. Xia. 2024. "Reconstruction for Beam Blockage of Lidar Based on Generative Adversarial Networks." *Optics Express* 32: 14420–14434.

Yuan, J., L. Su, H. Xia, et al. 2022. "Microburst, Windshear, Gust Front, and Vortex Detection in Mega Airport Using a Single Coherent Doppler Wind Lidar." *Remote Sensing* 14: 1626–1639.

Yuan, Y., P. Wang, D. Wang, and H. Jia. 2018. "An Algorithm for Automated Identification of Gust Fronts From Doppler Radar Data." *Journal of Meteorological Research* 32: 444–455.

Zhang, H., S. Wu, Q. Wang, B. Liu, B. Yin, and X. Zhai. 2019. "Airport Low-Level Wind Shear Lidar Observation at Beijing Capital International Airport." *Infrared Physics & Technology* 96: 113–122.

Zhao, S., and Y. Shan. 2022. "Study of the Algorithm for Wind Shear Detection With Lidar Based on Shear Intensity Factor." *Algorithms* 15: 133–147.

Zhao, S., C. Yang, Y. Shan, and F. Zhu. 2025. "Identification and Analysis of Wind Shear Within the Transiting Frontal System at Xining International Airport Using Lidar." *Remote Sensing* 17: 732–755.

Zhao, W. K., S. J. Zhao, Y. L. Shan, and X. J. Sun. 2021. "Numerical Simulation for Wind Shear Detection With a Glide Path Scanning Algorithm Based on Wind LiDAR." *IEEE Sensors Journal* 21: 20248–20257.

Zheng, J., J. Zhang, K. Z. Zhu, L. L. Liu, and Y. L. Liu. 2014. "Gust Front Statistical Characteristics and Automatic Identification Algorithm for CINRAD." *Journal of Meteorological Research* 28: 607–623.

Zhou, S., Y. Cui, H. Zheng, and T. Zhang. 2018. "Wind Shear Identification With the Retrieval Wind of Doppler Wearth Radar." *International Archives of the Photogrammetry, Remote Sensing and Spatial Information Sciences* XLII-3: 2553–2555.

Zrnić, D. S., D. W. Burgess, and L. D. Hennington. 1985. "Automatic Detection of Mesocyclonic Shear With Doppler Radar." *Journal of Atmospheric and Oceanic Technology* 2: 425–438.